

Appearance of T_d^* phase across the T_d - $1T'$ phase boundary in Weyl semimetal MoTe_2

Yu Tao,¹ John A. Schneeloch,¹ Chunruo Duan,¹ Masaaki Matsuda,² Sachith E. Dissanayake,^{2,*}
Adam A. Aczel,^{2,3} Jaime A. Fernandez-Baca,² Feng Ye,² and Despina Louca^{1,†}

¹*Department of Physics, University of Virginia, Charlottesville, Virginia 22904, USA*

²*Neutron Scattering Division, Oak Ridge National Laboratory, Oak Ridge, Tennessee 37831, USA*

³*Department of Physics and Astronomy, University of Tennessee, Knoxville, Tennessee 37996, USA*

Using elastic neutron scattering on single crystals of MoTe_2 and $\text{Mo}_{1-x}\text{W}_x\text{Te}_2$ ($x \lesssim 0.01$), the temperature dependence of the recently discovered T_d^* phase, present between the low temperature orthorhombic T_d phase and high temperature monoclinic $1T'$ phase, is explored. The T_d^* phase appears only on warming from T_d and is observed in the hysteresis region prior to the $1T'$ transition. This phase consists of four layers in its unit cell, and is constructed by an “AABB” sequence of layer stacking operations rather than the “AB” and “AA” sequences of the $1T'$ and T_d phases, respectively. Though the T_d^* phase emerges without disorder on warming from T_d , on cooling from $1T'$ diffuse scattering is observed that suggests a frustrated tendency toward the “AABB” stacking.

Many layered materials have structure-property relationships that depend on their layer stacking. For example, the transition metal dichalcogenide MoTe_2 is reported to be a type-II Weyl semimetal in its orthorhombic T_d phase (with the non-centrosymmetric $Pnm2_1$ space group) [1, 2], but not in its monoclinic $1T'$ phase (with the centrosymmetric space group $P2_1/m$). The two phases have nearly-identical layers and differ mainly by in-plane displacements. Though there is much interest in investigating Weyl semimetals, the properties of MoTe_2 are not completely understood. For instance, there is much debate on the origin of the extreme magnetoresistance observed at low temperatures [3–5], the number and location of Weyl points in the T_d phase [6], and the topological nature of the observed surface Fermi arcs that are a necessary but not sufficient condition for a Weyl semimetal [7]. Structural distortions have been known to occur, such as stacking disorder during the phase transition, evidenced by the presence of diffuse scattering observed in neutron [8] and X-ray [9] experiments, and hysteresis effects that extend far beyond the transition region, as seen in resistivity measurements along the thermal hysteresis loop [10]. These effects have been largely ignored, though one of the surface Fermi arcs was noted to persist to ~ 90 K above the transition temperature and to have a history-dependent appearance [6]. In general, structural phase transitions that involve in-plane translations of layers resulting from changes in temperature or pressure have been neglected, but many materials fall in this category, including Ta_2NiSe_5 [11], In_2Se_3 [12, 13], $\alpha\text{-RuCl}_3$ [14], CrX_3 ($X=\text{Cl, Br, I}$) [15], and MoS_2 [16–18]. A better understanding of these types of transitions would not only elucidate these material properties, but could also lead to the discovery of new phases.

The T_d and $1T'$ phases can be constructed from a stacking pattern of “A” and “B” operations, as shown in

Fig. 1(a). The A operation maps one layer of T_d to the layer below it, so T_d can be built from repeating “AA” sequences. The B operation is the same as for A but followed by a translation of ± 0.15 lattice units, with a sign that is alternating layer-by-layer. Thus, $1T'$ can be built from repeating “AB” sequences. We previously reported that diffuse scattering observed in the $H0L$ scattering plane on cooling from $1T'$ towards T_d (in particular, the low intensity along $(60L)$) is consistent with a disordered A/B stacking pattern [8]. How the stacking changes with temperature has not been closely examined, though an explanation for the relative stability of the T_d and $1T'$ phases via free energy calculations was earlier proposed [19]. Understanding the nature of layer stacking will provide useful insight into how Weyl nodes disappear across the phase boundary.

We performed elastic neutron scattering as a function of temperature to study the mechanism of the structural phase transition between the $1T'$ and T_d phases in MoTe_2 . On warming, the recently discovered T_d^* phase [20] was observed, having a pseudo-orthorhombic structure and a four-layer unit cell, rather than the two-layer unit cells of $1T'$ and T_d . The stacking sequence of T_d^* can be described by “AABB”, as shown in Fig. 1(a). Upon warming, the $T_d \rightarrow T_d^*$ transition is not accompanied by disorder. Diffuse scattering is observed on further warming from T_d^* to $1T'$. On the other hand, on cooling from $1T'$ to T_d , the T_d^* phase is absent and only diffuse scattering is observed that suggests a frustrated tendency toward the “AABB” layer order.

Elastic neutron scattering was performed at Oak Ridge National Laboratory, on the triple axis spectrometers HB1, CG4C, and HB1A at the High Flux Isotope Reactor; and on the time-of-flight spectrometer CORELLI at the Spallation Neutron Source [21]. Though the crystals are monoclinic at room temperature, for simplicity, we use orthorhombic coordinates, with $a \approx 6.3$ Å $b \approx 3.5$ Å and $c \approx 13.8$ Å. The collimations were $48'-40'-S-40'-120'$ for HB1 and CG4C, and $40'-40'-S-40'-80'$ for HB1A. Incident neutron energies were 13.5 meV for HB1, 4.5 meV for CG4C, and 14.6 meV for HB1A. Resistance mea-

* Present address: Duke University, Dept. of Physics, Durham, NC 27708

† Corresponding author. Email: louca@virginia.edu

measurements were performed in a Quantum Design Physical Property Measurement System. All crystals were grown in excess Te flux, including the two used for neutron scattering, “MT1” and “MT2”. MT1 has the composition MoTe_2 , while MT2 has the composition $\text{Mo}_{1-x}\text{W}_x\text{Te}_2$ with $x \lesssim 0.01$ as estimated by energy dispersive X-ray spectroscopy and the c -axis lattice constant. Details can be found in the Supplemental Materials.

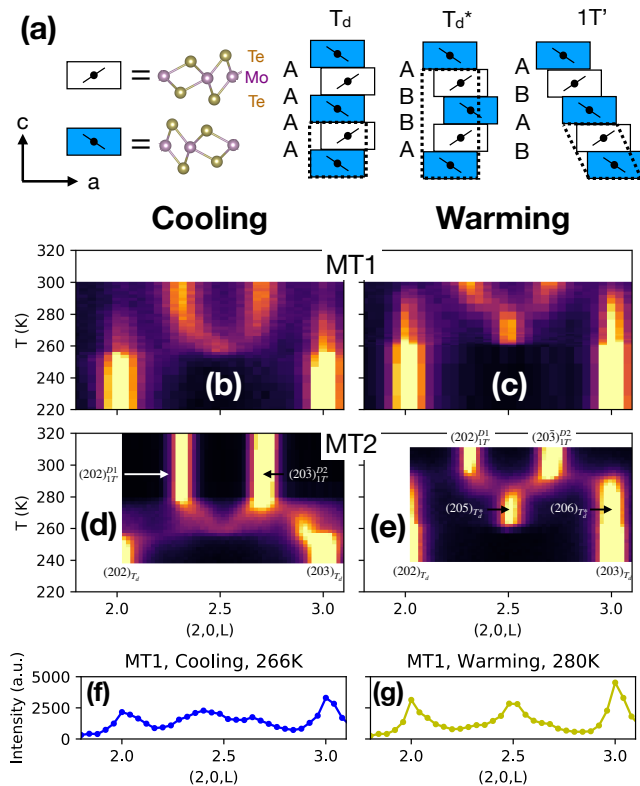


Figure 1. (a) The stacking patterns of $1T'$, T_d^* , and T_d . Rectangles show cells centered on points of inversion symmetry for each layer. Neutron scattering intensity maps for (b,c) MT1 and (d,e) MT2 as a function of temperature along the $(2,0,L)$ line on cooling (left) and warming (right). Data were taken on HB1A for (b,c) and HB1 for (d,e). (f,g) Intensity plots along $(2,0,L)$ showing diffuse scattering in MT1 on cooling (f) and warming (g).

In Figures 1(b-e), neutron scattering intensity scans along $(2,0,L)$ are combined for many temperatures on cooling and warming through the hysteresis. In the $1T'$ phase, the $(202)_{1T'}^{D1}$ and $(20\bar{3})_{1T'}^{D2}$ Bragg peaks are observed near $L = 2.3$ and $L = 2.7$, respectively; $D1$ and $D2$ denote each of the two $1T'$ twins. (Since MT1 could not be warmed fully into $1T'$ in Fig. 1(c) for technical reasons, diffuse scattering was present on subsequent cooling from 300 K in Fig. 1(b).) At low temperatures, T_d -phase Bragg peaks at $L = 2$ and $L = 3$ are observed, as indicated in the figure. On warming from T_d past ~ 260 K, a peak appears at $L = 2.5$, indicating the onset of T_d^* . The presence of this peak at half-integer L indicates an out-

of-plane doubling of the unit cell, so we label this peak $(205)_{T_d^*}$ (Fig. 1(e)). With additional warming, a gradual transformation into the $1T'$ phase occurs, accompanied by diffuse scattering indicating stacking disorder. Examples of the diffuse scattering can be seen in the individual plots of intensity along $(2,0,L)$ in Fig. 1(f), where $1T'$ is transitioning into T_d ; and in Fig. 1(g), where T_d^* is transitioning into $1T'$. For MT2, we measured through the hysteresis twice and found the same pattern of diffuse scattering at the same temperatures along the hysteresis, suggesting that the appearance of the diffuse scattering through the hysteresis is reproducible.

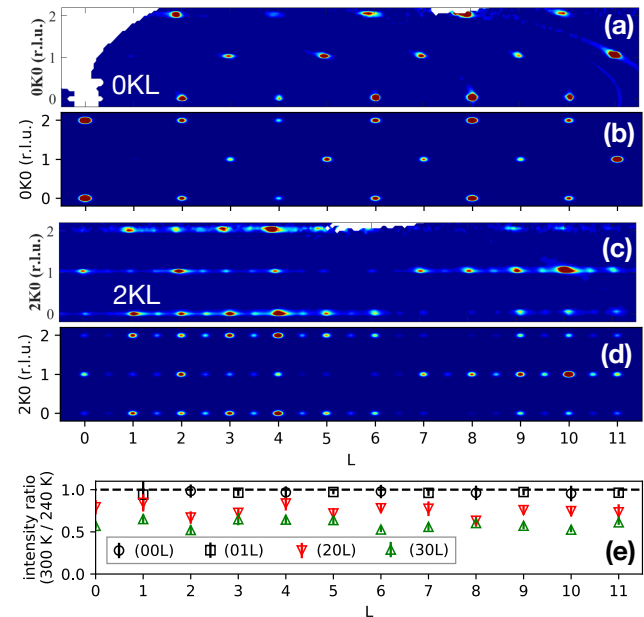


Figure 2. Neutron scattering intensity maps (a,c) and simulated data (b,d) in the OKL (a,b) and $2KL$ (c,d) scattering planes in the T_d^* phase from the MT1 crystal measured at CORELLI. Data taken on warming at 300 K. (e) Ratio of selected Bragg peak intensities between 300 K and 240 K. Intensities are from Gaussian fits from data averaged within ± 0.2 r.l.u. in the H - and K -directions.

The T_d^* phase structure can be deduced from the following observations: First, T_d^* appears to be orthorhombic, but has additional peaks at half-integer L values relative to T_d , indicating a four-layer unit cell. Second, the $1T'$ and T_d phases can be built from A/B stacking sequences, so we presume the same is true for T_d^* . There are only two possible pseudo-orthorhombic stacking sequences: “AABB” and “ABBA”, which are twins of each other. Since this structure, with highest possible symmetry $P2_1/m$, appears to have an orthorhombic unit cell but has atomic positions incompatible with orthorhombic space groups, we refer to it as pseudo-orthorhombic.

To verify the predicted AABB stacking structure of T_d^* , we carried out single-crystal neutron diffraction measurements on the MT1 crystal on CORELLI, and the data are

shown in Figures 2(a,c). The data were taken on warming to 300 K, and the presence of peaks at half-integer L in the $2KL$ plane in Fig. 2(c) confirm the presence of the T_d^* phase. The diffuse scattering streaks along L are from stacking disorder that was already present on warming from 240 K, possibly due to not cooling sufficiently into T_d beforehand. (There is a discrepancy between the detection of T_d^* in MT1 at 300 K on CORELLI and up to ~ 280 K on HB1A. The cause of the temperature discrepancy is unknown, but may be related to the presence of stacking disorder before warming.) Figures 2(b,d) show simulated intensity maps. To match the data, it was necessary to consider a 47.8% volume fraction of T_d as well as 28.2% and 24.0% volume fractions of the two T_d^* twins. The volume fractions were obtained by fitting the intensities of Bragg peaks within $-1 \leq H \leq 8$, $-1 \leq K \leq 1$, and $-20 \leq L \leq 20$ with the calculated peak intensities of the ideal “AA”, “AABB”, and “ABBA” stacking sequences of T_d and the two T_d^* twins, respectively. These structures were built from layers having the coordinates in Ref. [22]. As can be seen in Figures 2(a-d), the patterns of peak intensities in these scattering planes match those arising from our model.

Stringent constraints on possible T_d^* structures follow from the lack of change in $(00L)$ and $(01L)$ peak intensities between the T_d phase at 240 K and the T_d^* phase at 300 K (as seen from the near-unity intensity ratios in Fig. 2(e). For context, intensity ratios for $(20L)$ and $(30L)$ peaks are also included.) A lack of change in $0KL$ peak intensities implies a lack of change in atomic positions along the b - and c -directions, but is consistent with layer displacements along the a -direction, as is the case between $1T'$ and T_d [8]. The AABB structure should be centrosymmetric, since it can be transformed from the centrosymmetric AB-stacked $1T'$ phase by a centrosymmetric series of translations (see Supplementary Materials). Inversion symmetry centers for the AABB structure are depicted in Fig. S2 in the Supplemental Materials. Barring small non-centrosymmetric distortions, which are unlikely given that first-principles calculations have shown that MoTe_2 layers isolated from the non-centrosymmetric T_d environment tend to become centrosymmetric [23], we conclude that T_d^* is centrosymmetric with $P2_1/m$ symmetry. A structural refinement assuming $P2_1/m$ symmetry was performed (see Supplementary Materials), with rough agreement between the refined and ideal coordinates, though the absence of visible $0KL$ peaks in our data (apart from those with even $K + L$) indicates that the true T_d^* structure is closer to the ideal AABB stacking than our refined coordinates.

For a closer look at how the transition proceeds, in Fig. 3(a,b) we plot intensities for four Bragg peaks as a function of temperature. The integrated intensities were obtained from fits of the data shown in Figures 1(d) and 1(e). On cooling below ~ 280 K (Fig. 3(a)), there is a steady decrease in the intensity of the $1T'$ peaks in the hysteresis region. The peaks eventually become difficult to resolve from the diffuse scattering, and fitting was not

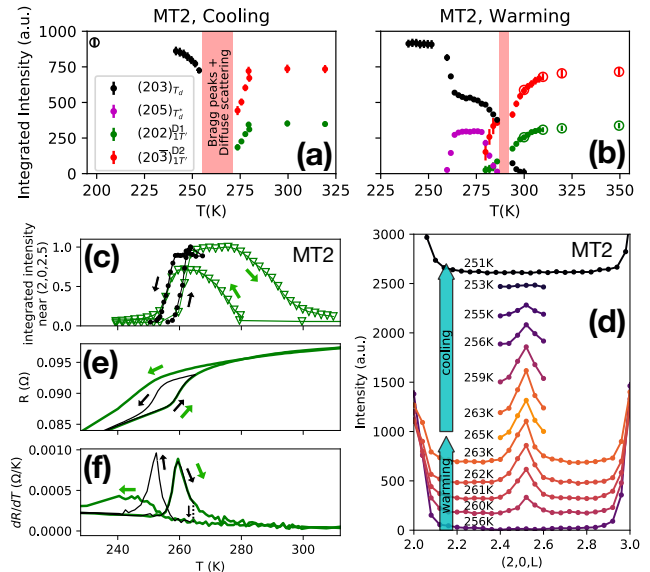


Figure 3. (a,b) Bragg peak intensities plotted as a function of temperature on warming and cooling for MT2. Red bands denote regions where fitting was poor. Closed symbols denote fits to the same hysteresis loop (with cooling data measured before warming). Open symbols correspond to a previous hysteresis loop. (c) Plots of intensity integrated within $(2, 0, 2.39 \leq L \leq 2.61)$ for MT2 taken through two different hysteresis loops. Data taken on CG4C for the narrow hysteresis (black), and on HB1 for the wide hysteresis (green; from same data as Fig. 1(d,e).) Curves normalized to their largest values. (d) Neutron scattering intensity along $(2, 0, L)$ for MT2, with data taken on CG4C at various temperatures, vertically displaced for clarity. (e) Resistance of a MoTe_2 crystal, measured through two hysteresis loops that begin on warming from 200 K. (f) The derivative dR/dT of the data shown in (e).

done within the region indicated by the pink shaded bar. On further cooling, the T_d peaks appear.

In contrast, on warming the intensities of the T_d peaks in Fig. 3(b) remain constant until a sudden change is observed around 260 K. At this temperature, the T_d^* peaks appear (magenta symbols) at the expense of the T_d peaks. On further warming, the T_d and T_d^* peak intensities both decrease and disappear by 280 K. Again, diffuse scattering is observed (pink shaded region) prior to the crystal transforming fully into $1T'$. Though a coherent, long-range T_d^* phase only appears on warming, the intensity shift toward $(2, 0, 2.5)$ on cooling as seen in Fig. 1(b) and 1(d) suggests a tendency toward the AABB stacking, though frustrated and not resulting in an ordered structure. On both cooling into T_d or warming into $1T'$, there is a gradual increase in the intensity of the T_d and $1T'$ peaks, which occurs with a decrease in diffuse scattering (see Fig. S3 of the Supplemental Materials). This lingering diffuse scattering is probably related to the long residual hysteresis commonly observed

in the resistivity measurements (e.g., in Ref. [24], or Fig. S4 in the Supplemental Materials.)

To investigate the boundary between the T_d and T_d^* regions, in Fig. 3(c), intensity integrated near $(2, 0, 2.5)$ is plotted for two different thermal hysteresis loops for the MT2 crystal. The narrow hysteresis loop (black symbols) corresponds to the sample warming into T_d^* , then cooling back to T_d without entering $1T'$. Fig. 3(d) is a plot of the data used to calculate the narrow hysteresis loop intensities. The $(205)_{T_d^*}$ peak intensity rises and falls through the hysteresis loop. Diffuse scattering is not present even at a temperature a few Kelvin below the T_d^* peak's disappearance on cooling. Thus, $T_d^* \rightarrow T_d$ likely proceeds without disorder. In contrast, a wider hysteresis loop (green symbols) is observed when the sample is allowed to warm into $1T'$. This is coupled to the substantial diffuse scattering present on cooling, as shown earlier in Fig. 1(d,e). Nevertheless, for both narrow and wide hysteresis loops, a sudden drop of intensity near $(2, 0, 2.5)$ appears on cooling below 255 K, though more gradually for the wide hysteresis loop.

A similar pattern can be seen in the resistance data of Fig. 3(e), taken on a MoTe_2 crystal with residual resistance ratio ~ 460 through consecutive narrow (black; 200 to 265 K) and wide (green; 200 to 350 K) hysteresis loops. On cooling, the resistance decreases quickly and in a symmetric manner (for cooling vs. warming) for the narrow hysteresis loop, but more slowly and asymmetric for the wide hysteresis loop. Even so, the temperature at which both loops begin to bend on cooling is similar, as seen from dR/dT in Fig. 3(f), though slightly lower for the wide hysteresis loop. The kink seen on warming (near 258 K) is likely the onset of T_d^* and not $1T'$, judging from the temperature and the similarities between the resistance and neutron scattering hysteresis loops.

We next discuss how these structural transitions proceed and the kinds of interlayer interactions that may be responsible, beginning from the observation that the onset to T_d occurs at a similar temperature whether cooling from the ordered T_d^* phase, or from the frustrated T_d^* region accessed on cooling from $1T'$. Since the onset temperature to T_d does not appear to vary substantially with overall stacking disorder, we suggest that *short-range* rather than long-range interlayer interactions determine the onset temperatures (into $1T'$ or T_d^* as well as T_d). (Though we use the term “interlayer interactions”, we emphasize that these are effective interactions. Whether an interlayer boundary shifts from A \rightarrow B depends on the free energy, which depends on the surrounding environment, which is specified by the A/B stacking sequence. “Interlayer interactions” represent the dependence of an interlayer boundary’s contribution to the free energy on the surrounding stacking, and can be indirect, involving changes to band structure, phonon dispersion, etc.)

In contrast, *long-range* interlayer interactions may govern the gradual decrease in diffuse scattering and increase in Bragg peak intensities on warming into $1T'$

or cooling into T_d . What kind of stacking faults causing this diffuse scattering persist on cooling into T_d , even when short-range interlayer interactions favor an ordered phase? At twin boundaries, shifts of A \rightarrow B or B \rightarrow A (e.g., AAAABBB... \rightarrow AAABBBB...) would not change the short-range environment, and could only be induced by changes in long-range interlayer interactions. The decrease in diffuse scattering in T_d on cooling can be explained by the annihilation of these twin boundaries, either by joining in pairs or by exiting a crystal surface. The lack of change on subsequent warming can be explained by the relaxation of conditions that, on cooling, had driven twin boundaries to annihilate.

Previous studies on MoTe_2 should be re-examined in light of the existence of the T_d^* phase. First, the hysteresis loop in resistivity (first reported in Ref. [25]) has been interpreted as indicating the transition between T_d and $1T'$, but in view of the current data, most of the change in the resistance occurs between T_d and T_d^* on warming. Second, second harmonic generation (SHG) intensity measurements, expected to be zero for inversion symmetry and nonzero otherwise, show abrupt (within <4 K) changes on both heating and cooling through the hysteresis loop [26]. Since the transition to $1T'$ occurs gradually, and since T_d^* appears to be centrosymmetric, the abrupt warming transition seen in SHG may be due to the $T_d \rightarrow T_d^*$ rather than $T_d \rightarrow 1T'$ transition. The abrupt transition on cooling is harder to explain, but it is possible that the loss of inversion symmetry on cooling into T_d occurs suddenly even as the transition proceeds with disorder. Our findings may also inform proposed applications, such as the photoinduced ultrafast topological switch in Ref. [27]; since the $T_d \rightarrow T_d^* \rightarrow T_d$ transition occurs without disorder and with only a ~ 5 K hysteresis, and since T_d^* appears to be centrosymmetric, a topological switch may more efficiently use T_d^* rather than $1T'$.

In conclusion, using elastic neutron scattering, we mapped the changes in stacking that occur in the thermal hysteresis between the T_d and $1T'$ phases in MoTe_2 . On warming from the orthorhombic T_d , T_d^* arises without diffuse scattering and corresponds to an “AABB” sequence of stacking operations. Diffuse scattering is present on further warming from T_d^* to $1T'$, and on cooling from $1T'$ to T_d , where a frustrated tendency toward the “AABB” stacking is seen. Thus, the $1T'$ - T_d transition has complex structural behavior and deserves further study.

ACKNOWLEDGEMENTS

This work has been supported by the Department of Energy, Grant number DE-FG02-01ER45927. A portion of this research used resources at the High Flux Isotope Reactor and the Spallation Neutron Source, which are DOE Office of Science User Facilities operated by Oak Ridge National Laboratory.

- [1] Y. Sun, S.-C. Wu, M. N. Ali, C. Felser, and B. Yan, “Prediction of Weyl semimetal in orthorhombic MoTe_2 ,” *Phys. Rev. B* **92**, 161107(R) (2015).
- [2] K. Deng, G. Wan, P. Deng, K. Zhang, S. Ding, E. Wang, M. Yan, H. Huang, H. Zhang, Z. Xu, *et al.*, “Experimental observation of topological fermi arcs in type-II Weyl semimetal MoTe_2 ,” *Nature Physics* **12**, 1105 (2016).
- [3] D. Rhodes, R. Schönemann, N. Aryal, Q. Zhou, Q. R. Zhang, E. Kampert, Y.-C. Chiu, Y. Lai, Y. Shimura, G. T. McCandless, J. Y. Chan, D. W. Paley, J. Lee, A. D. Finke, J. P. C. Ruff, S. Das, E. Manousakis, and L. Balicas, “Bulk Fermi surface of the Weyl type-II semimetallic candidate γ - MoTe_2 ,” *Phys. Rev. B* **96**, 165134 (2017).
- [4] Q. Zhou, D. Rhodes, Q. R. Zhang, S. Tang, R. Schönemann, and L. Balicas, “Hall effect within the colossal magnetoresistive semimetallic state of MoTe_2 ,” *Phys. Rev. B* **94**, 121101(R) (2016).
- [5] S. Thirupathaiah, R. Jha, B. Pal, J. S. Matias, P. K. Das, P. K. Sivakumar, I. Vobornik, N. C. Plumb, M. Shi, R. A. Ribeiro, and D. D. Sarma, “ MoTe_2 : An uncompensated semimetal with extremely large magnetoresistance,” *Phys. Rev. B* **95**, 241105(R) (2017).
- [6] A. P. Weber, P. Rießmann, N. Xu, S. Muff, M. Fanciulli, A. Magrez, P. Bugnon, H. Berger, N. C. Plumb, M. Shi, S. Blügel, P. Mavropoulos, and J. H. Dil, “Spin-Resolved Electronic Response to the Phase Transition in MoTe_2 ,” *Phys. Rev. Lett.* **121**, 156401 (2018).
- [7] N. Xu, Z. W. Wang, A. Magrez, P. Bugnon, H. Berger, C. E. Matt, V. N. Strocov, N. C. Plumb, M. Radovic, E. Pomjakushina, K. Conder, J. H. Dil, J. Mesot, R. Yu, H. Ding, and M. Shi, “Evidence of a Coulomb-Interaction-Induced Lifshitz Transition and Robust Hybrid Weyl Semimetal in T_d - MoTe_2 ,” *Phys. Rev. Lett.* **121**, 136401 (2018).
- [8] J. A. Schneeloch, C. Duan, J. Yang, J. Liu, X. Wang, and D. Louca, “Emergence of topologically protected states in the MoTe_2 Weyl semimetal with layer-stacking order,” *Phys. Rev. B* **99**, 161105(R) (2019).
- [9] R. Clarke, E. Marseglia, and H. P. Hughes, “A low-temperature structural phase transition in β - MoTe_2 ,” *Philos. Mag. B* **38**, 121–126 (1978).
- [10] T. Zandt, H. Dwelk, C. Janowitz, and R. Manzke, “Quadratic temperature dependence up to 50?K of the resistivity of metallic MoTe_2 ,” *J. Alloys Compd. Proceedings of the 15th International Conference on Solid Compounds of Transition Elements*, **442**, 216–218 (2007).
- [11] A. Nakano, K. Sugawara, S. Tamura, N. Katayama, K. Matsubayashi, T. Okada, Y. Uwatoko, K. Munakata, A. Nakao, H. Sagayama, R. Kumai, K. Sugimoto, N. Maejima, A. Machida, T. Watanuki, and H. Sawa, “Pressure-induced coherent sliding-layer transition in the excitonic insulator Ta_2NiSe_5 ,” *IUCrJ* **5** (2018), 10.1107/S2052252517018334.
- [12] F. Ke, C. Liu, Y. Gao, J. Zhang, D. Tan, Y. Han, Y. Ma, J. Shu, W. Yang, B. Chen, H.-K. Mao, X.-J. Chen, and C. Gao, “Interlayer-glide-driven isosymmetric phase transition in compressed In_2Se_3 ,” *Appl. Phys. Lett.* **104**, 212102 (2014).
- [13] Jinggeng Zhao and Liuxiang Yang, “Structure Evolutions and Metallic Transitions in In_2Se_3 Under High Pressure,” *J. Phys. Chem. C* **118**, 5445–5452 (2014).
- [14] A. Glamazda, P. Lemmens, S.-H. Do, Y. S. Kwon, and K.-Y. Choi, “Relation between Kitaev magnetism and structure in α - RuCl_3 ,” *Phys. Rev. B* **95**, 174429 (2017).
- [15] M. A. McGuire, H. Dixit, V. R. Cooper, and B. C. Sales, “Coupling of Crystal Structure and Magnetism in the Layered, Ferromagnetic Insulator CrI_3 ,” *Chem. Mater.* **27**, 612–620 (2015).
- [16] L. Hromadová, R. Martoňák, and E. Tosatti, “Structure change, layer sliding, and metallization in high-pressure MoS_2 ,” *Phys. Rev. B* **87**, 144105 (2013).
- [17] Z.-H. Chi, X.-M. Zhao, H. Zhang, A. F. Goncharov, S. S. Lobanov, T. Kagayama, M. Sakata, and X.-J. Chen, “Pressure-Induced Metallization of Molybdenum Disulfide,” *Phys. Rev. Lett.* **113**, 036802 (2014).
- [18] A. P. Nayak, S. Bhattacharyya, J. Zhu, J. Liu, X. Wu, T. Pandey, C. Jin, A. K. Singh, D. Akinwande, and J.-F. Lin, “Pressure-induced semiconducting to metallic transition in multilayered molybdenum disulphide,” *Nat. Commun.* **5**, 3731 (2014).
- [19] H.-J. Kim, S.-H. Kang, I. Hamada, and Y.-W. Son, “Origins of the structural phase transitions in MoTe_2 and WTe_2 ,” *Phys. Rev. B* **95**, 180101(R) (2017).
- [20] S. Dissanayake, C. Duan, J. Yang, J. Liu, M. Matsuda, C. Yue, J. A. Schneeloch, J. C. Y. Teo, and D. Louca, “Electronic band tuning under pressure in MoTe_2 topological semimetal,” *npj Quantum Mater.* **4**, 1–7 (2019).
- [21] F. Ye, Y. Liu, R. Whitfield, R. Osborn, and S. Rosenkranz, “Implementation of cross correlation for energy discrimination on the time-of-flight spectrometer CORELLI,” *J. Appl. Crystallogr.* **51**, 315–322 (2018).
- [22] Y. Qi, P. G. Naumov, M. N. Ali, C. R. Rajamathi, W. Schnelle, O. Barkalov, M. Hanfland, S.-C. Wu, C. Shekhar, Y. Sun, V. Süß, M. Schmidt, U. Schwarz, E. Pippel, P. Werner, R. Hillebrand, T. Förster, E. Kampert, S. Parkin, R. J. Cava, C. Felser, B. Yan, and S. A. Medvedev, “Superconductivity in Weyl semimetal candidate MoTe_2 ,” *Nat. Commun.* **7**, 11038 (2016).
- [23] C. Heikes, I.-L. Liu, T. Metz, C. Eckberg, P. Neves, Y. Wu, L. Hung, P. Piccoli, H. Cao, J. Leao, J. Paglione, T. Yildirim, N. P. Butch, and W. Ratcliff, “Mechanical control of crystal symmetry and superconductivity in Weyl semimetal MoTe_2 ,” *Phys. Rev. Mater.* **2**, 074202 (2018).
- [24] T. Zandt, H. Dwelk, C. Janowitz, and R. Manzke, “Quadratic temperature dependence up to 50 k of the resistivity of metallic MoTe_2 ,” *J. Alloys Compd.* **442**, 216–218 (2007).
- [25] H. P. Hughes and R. H. Friend, “Electrical resistivity anomaly in β - MoTe_2 ,” *J. Phys. C: Solid State Phys.* **11**, L103 (1978).
- [26] H. Sakai, K. Ikeura, M. S. Bahramy, N. Ogawa, D. Hashizume, J. Fujioka, Y. Tokura, and S. Ishiwata, “Critical enhancement of thermopower in a chemically tuned polar semimetal MoTe_2 ,” *Sci. Adv.* **2**, e1601378 (2016).
- [27] M. Y. Zhang, Z. X. Wang, Y. N. Li, L. Y. Shi, D. Wu, T. Lin, S. J. Zhang, Y. Q. Liu, Q. M. Liu, J. Wang, T. Dong, and N. L. Wang, “Light-Induced Subpicosecond Lattice Symmetry Switch in MoTe_2 ,” *Phys. Rev. X* **9**, 021036 (2019).